Plant Soil (2013) 373:157–171
DOI 10.1007/s11104-013-1768-z

REGULAR ARTICLE

Biochemical characterization of cell types within leaves of metal-hyperaccumulating *Noccaea praecox* (Brassicaceae)

Marjana Regvar · Diane Eichert · Burkhard Kaulich · Alessandra Gianoncelli · Paula Pongrac · Katarina Vogel-Mikuš

Received: 22 March 2013 / Accepted: 8 May 2013 / Published online: 7 June 2013

Abstract
Background and aims Distinct metal distribution patterns within leaves of metal hyperaccumulating plants are repeatedly observed however, the presumable role of key structural biochemical molecules in determining and regulating their allocation remains largely unknown. We aimed to characterise in a spatially resolved manner the distribution of the main biochemical components in leaves of field-collected Cd/Zn-hyperaccumulating *Noccaea praecox* in order to relate them to metal distribution patterns at tissue level.
Methods The biomolecular composition of the leaves was spatially analysed using synchrotron radiation Fourier Transform Infrared (FTIR) and the distribution of Zn with synchrotron radiation Low-Energy X-Ray Fluorescence (LEXRF) microspectroscopy was determined on the same tissues of interest (epidermis, subepidermis, mesophyll).
Results In epidermal cells high proportion of free-carboxyl, nitro and phosphate groups standing for pectin, nitroaromatics, phytic and other organic acids were found. Adjacent mesophyll cells had higher proportions of proteins, carbohydrates and cellulosic compounds.
Conclusions Pectin compounds were indicated as important components of Zn enriched epidermal cell walls. In addition, intense lignification of epidermal cell walls might limit leakage of the trapped metals back to the metabolically active and thus more sensitive mesophyll. Distribution of metal-binding compounds in particular cell types/tissues may therefore predispose metal distribution patterns and tolerance in leaves.

Keywords *Noccaea* (formerly *Thlaspi*) *praecox* · Synchrotron radiation Fourier transform infrared (FTIR) · Synchrotron radiation low-energy X-ray fluorescence (LEXRF) · Carbohydrate · Egg-box model · Pectin · Zn

Responsible Editor: Juan Barcelo.

M. Regvar (✉) · P. Pongrac · K. Vogel-Mikuš
Department of Biology, Biotechnical Faculty,
University of Ljubljana,
Večna pot 111,
1000 Ljubljana, Slovenia
e-mail: marjana.regvar@bf.uni-lj.si

P. Pongrac
e-mail: paula.pongrac@bf.uni-lj.si

K. Vogel-Mikuš
e-mail: katarina.vogel@bf.uni-lj.si

D. Eichert · B. Kaulich · A. Gianoncelli
Elettra-Sincrotrone Trieste,
S.S. 14 Km 163.5 in Area Science Park,
34149 Basovizza, Trieste, Italy

D. Eichert
e-mail: diane.eichert@elettra.eu

B. Kaulich
e-mail: burkhard.kaulich@diamond.ac.uk

A. Gianoncelli
e-mail: alessandra.gianoncelli@elettra.trieste.it

Present Address:
B. Kaulich
Diamond Light Source Ltd,
Diamond House, Harwell Science and Innovation Campus,
Didcot, Oxfordshire OX11 0DE, UK

Introduction

Metal hyperaccumulating plants are defined by high metal concentrations in leaves and efficient metal tolerance mechanisms. Their distinct mechanisms of metal homeostasis represent the basic physiological background that enables them to cope with accumulated metals, involving coordination of metal-ion transporters and ligands that participate in metal uptake, translocation and compartmentalisation at the tissue and cellular levels (Haydon and Cobbett 2007). Metal transport in hyperaccumulating plants is characterised by stimulated metal influx across the root-cell plasma membrane, reduced metal sequestration in the root vacuoles, increased loading of metals into the xylem for transport to the leaves, stimulated metal influx across the leaf-cell plasma membrane, and increased metal sequestration in the leaf-cell vacuoles (Rascio and Navari-Izzo 2011). In leaves effective coordination and transfer between different cell types is required to control the storage of the high metal concentrations. In the metal-hyperaccumulating *Noccaea* (formerly *Thlaspi*) species the highest metal concentrations were found in leaf epidermal cells (Küpper et al. 1999; Vogel-Mikuš et al. 2008a, b), which indicate a way to avoid perturbation of photosynthesis processes (Milner and Kochian 2008). Nevertheless a significant fraction of the total leaf metal accumulation occurs also in the mesophyll, as the mesophyll constitutes a large fraction of the leaf biomass (Ma et al. 2005; Milner and Kochian 2008).

At the leaf cellular and sub-cellular levels, storage in the vacuole (via weak oxygen ligands such as organic acids) and metal immobilisation within the cell through binding to different ligands in the cytosol is a predominant tolerance mechanism (Salt et al. 1999; McNear et al. 2010). A significant amount of metals can also be detected in the apoplast, indicating that cell wall components also have an important role in metal homeostasis (Küpper et al. 1999, 2004; Vogel-Mikuš et al. 2008b). Nonetheless, the role of the apoplast in metal transport, distribution and immobilisation within leaves of metal-hyperaccumulating plants is poorly understood (Milner and Kochian 2008). In other organisms such as brown algae (Andrade et al. 2010) and moss *Pohlia drummondii* (Lang and Wernitznig 2011) sequestration of metals in the cell wall is a key mechanism conferring metal tolerance. The structural components of cell walls have negatively charged surfaces that lead to accumulation of cations and repulsion of anions due to electrostatic interactions (Mari and Lebrun 2005). The structure of the chain aggregates that arise from their geometry for the accommodation of the divalent cations in-between (especially Ca) has been described as the 'egg-box' model (Grant et al. 1973). However, the relationship between cell wall structures and diverse cellular biological events from one side, and their relation with the emerging understanding of polymer functions remains to be unravelled (Knox 2008).

One of the major obstacles in studies of evaluation of the metal affinity to the cell wall components is in poor sensitivity of the available techniques. An additional drawback is that these techniques rely on bulk analysis, which is hampered by the clear potential for compartment mixing and degradation or transformation of the components, thus not allowing the specification of which tissues (e.g. epidermis or mesophyll) or cell compartments (e.g. cell wall, vacuoles or cytoplasm) the metal-ligand complexes were derived from. Therefore there is an increasing need to develop technology for systems-level analysis of specific cell types (Wang et al. 2012), ideally non-invasive and non-destructive, to enable the precise identification of the spatial partitioning of ligands involved in chelation of the metal ions between and within tissues (Mari and Lebrun 2005). One of such techniques is synchrotron radiation Fourier-transform infrared (FTIR) microspectroscopy which provides reliable information on the biochemical composition (molecules) in a spatially resolved manner. Infrared radiation does not cause any radiation damage to biological material as it can probe the chemical nature of the sample constituents without breaking the chemical bonds (Wetzel et al. 1998; Miller and Dumas 2006). Therefore the same material, even the same cells, can be subsequently used for determining the spatial distribution of elements using complementary techniques such as synchrotron radiation low-energy X-ray fluorescence (LEXRF) microspectroscopy (Ide-Ektessabi 2007; Kaulich et al. 2009). Such multi-methods approach (Eichert et al. 2007) allows highly sensitive, multi-element and multi-molecular, i.e. biochemical analyses of plant tissues in situ, and is therefore essential for an accurate representation and comprehension of the microstructure composition of the plant leaves.

Tolerance of plant populations to metal levels in excess is evolutionary achieved by adaptations resulting from increased physiological efficiency that is defined

by traits specific to each plant (Ernst 2006). We hypothesise that specific features contributing to metal tolerance of the metal-enriched leaf epidermal cells in field-collected Cd/ Zn hyperaccumulating *N. praecox* are resembled in the presence of functional groups of biomolecules (e.g. -COOH, -OH, -SH, -PO4) involved in metal immobilisation. In order to determine biomolecular and elemental composition of different tissues (epidermis, subepidermis and mesophyll) in the leaves these two techniques (FTIR and LEXRF) were used on the same area of interest. Potential relationships between biomolecular compositions with metal (primarily Zn) localization in particular leaf cell types are discussed.

Materials and methods

Plant sample preparation

Completely developed specimens of *Nocceae praecox* were collected at Žerjav, a site of high Cd, Zn and Pb metal pollution in Slovenia (P3: 46° 28′ 26.5″ N; 14° 51′ 56.0″ E) which detailed soil metal concentrations were previously reported and bulk analysis of the leaves of plants in vegetative growth phase revealed the following concentrations for Zn, Cd, Ni and Pb: 1,099±117, 867±41, 8.0±1.3 and 2,987±485 mg kg^{-1}, respectively (Pongrac et al. 2007). The plants were maintained in original soil in a growing chamber (16 h day period, 20 °C, 75 % relative humidity and 200 μmol m^{-2} s^{-1} photon flux density) and watered with distilled water for further two weeks until sampled. At sampling, intact, fully developed rosette leaves of adult plants, matured before transplanting, were selected. For the studies of morphological characteristics the fully developed rosette leaves were hand cut and hand cross-sections were examined under light microscope using visible light and UV (365 nm) excitation. For the plant analyses using FTIR and LEXRF 5×2 mm leaf pieces were excised using a razor blade from the leaf mid-rib area (as illustrated in Vogel-Mikuš et al. 2008a), mounted into stainless steel needles and immediately plunge-frozen in liquid propane cooled with liquid nitrogen (Vogel-Mikuš et al. 2009). Because plant leaves have poor temperature conductivity, cutting the leaf to smaller pieces was necessary to retain high freezing speed which minimizes the growth of ice crystals in the cells (Schneider et al. 2002). The whole procedure was performed quickly in order to minimize redistribution of the solutes within the tissues. Deeply frozen leaf pieces were transferred to a Leica CM3050 cryotome (Leica, Germany) chamber in a liquid-nitrogen-cooled thermoblock, to avoid thawing of the samples and mounted onto cryotome head. The temperature of the cryotome head and the chamber varied from −30 to −25 °C. At the beginning of the sectioning initial few 60 μm thin sections were cut off and discarded to avoid possible artefacts such as drainage of the cell components during leaf piece excision. The leaves were sectioned to 12 μm in order to avoid saturation of FTIR spectra when collected in transmission mode. The sections were placed onto specially pre-cooled aluminium containers and covered with flat stainless steel lid to ensure the flatness of the sections, transferred to an Alpha 2–4 Christ freeze-dryer (Martin Christ Gefriertrocknungsanlagen GmbH, Germany) via a cryo-transfer assembly cooled with liquid nitrogen, and freeze-dried at temperatures increasing from −80 to −25 °C, with a pressure of 0.34 mbar for 3 days. Freeze-drying procedure with slow increases in temperature to a great extent limits plasmolysis and deformation of morphological structures, as ice crystals that might have formed during freezing procedure are slowly sublimated. Ice crystal sublimation (not water evaporation) prevents the redistribution of elements and adsorption of cytosolic components by the cell wall areas during drying (Schneider et al. 2002; Vogel-Mikuš et al. 2009). Dried leaf cross-sections were placed between transmission electron microscopy gold grids, allowing correlated FTIR and LEXRF investigations of the same specimen and over the same areas of interest.

Scanning area and sample statistics

Synchrotron radiation based FTIR and LEXRF were applied to the same areas and cells of interest on two independent leaf samples (areas of about 60×60 μm containing approximately 14 cells each) to ensure the reliability and representativeness of the data. In addition, using FTIR, two additional maps, one per sample were acquired in the region of lower epidermis, and numerous point spectra (altogether 100) were collected on features of interest for statistical purposes. Moreover, FTIR imaging of further two specimens was performed using a conventional source coupled

with a focal plane array detector, which allows for probing a sample area of 170×170 μm (around 130 cells, 2 maps each), to confirm the results. The conclusions were drawn on the basis of all the results obtained for each particular tissue type but only the representative maps of the specimen acquired successively with synchrotron radiation FTIR and LEXRF on the very same cells of interest, were selected for presentation in the figures.

Synchrotron radiation FTIR microspectroscopy

The measurements were carried on at the SISSI infrared beamline at Elettra - Sincrotrone Trieste (Lupi et al. 2007; Eichert et al. 2008). The spectra were collected using a Bruker Vertex 70 interferometer coupled with a visible/ infrared Bruker Hyperion 3000 microscope, a single point HgCdTe (MCT) detector and a KBr beam splitter (Bruker Optic, Germany). The bench was configured to use collimated synchrotron light, a necessary condition for high-resolution imaging (Wetzel et al. 1998; Miller and Dumas 2006). The infrared spectra were acquired in transmission, at room temperature, in the 4,000–800 cm^{-1} region, after 512 co-added scans at 4 cm^{-1} spatial resolution, with a X15 infrared objective and Schwarzschild condenser, and apertures settings of 5×5 μm or 10×10 μm. Background spectra were collected every 10 points in an area free of sample, to compensate for variations in the atmospheric environment as well as for decay in intensity of the synchrotron source. All of the spectra were analysed with the OPUS NT 6.5 software package (Bruker). Briefly, each raw spectrum was systematically corrected for interference due to any atmospheric environment changes, truncated to a range of 3,800–800 cm^{-1}, smoothed using a Savitzky Golay algorithm (9 points), and baseline corrected using a concave Rubberband algorithm (64 points, 5 iterations). Chemical functional groups images were generated by plotting the intensities of the synchrotron infrared absorption bands as functions of their plane position, with a step size of 5 μm. For accurate comparison of the different spectral domain and their intensity, the spectra were normalised using a vector-normalisation algorithm within the energy range of interest, removing possible effect of thickness or baseline changes in the spectra resulting from light scattering effect.

Synchrotron-radiation-based X-ray microscopy and low-energy X-ray fluorescence (LEXRF) microspectroscopy

The synchrotron radiation X-ray-scanning transmission and LEXRF micro-spectroscopy analyses were conducted on the TwinMic endstation at Elettra-Sincrotrone Trieste (Italy) (Kaulich et al. 2006). TwinMic is a multipurpose soft X-ray transmission and emission microscope, which operates in the 400 eV to 2,200 eV energy range, and which combines X-ray transmission imaging with morphological and structural analyses of specimens in absorption and phase contrast modes and element and chemical micro-spectroscopy analyses employing LEXRF mode. A tunable, monochromatic X-ray beam extracted from a short undulator X-ray source was focused on a spot of approximately 1 μm in diameter using a tungsten zone plate (www.zoneplates.com) of 320 μm diameter and 50 nm outermost zone width. An incident photon energy of 1,216 eV was chosen to excite the K and L edges of elements with atomic numbers between Z=5–11 and Z=20–32, respectively. This low X-ray energy range (Kaulich et al. 2009) is of particular interest for biological samples, as it allows simultaneous access to very low Z elements (C, N and O), and therefore to the carbon-based skeleton of tissues, and to higher Z elements, through their L and M emission lines, which represent signatures of physiologically important macro, micro and trace elements. However, with this excitation energy, other biologically important elements were out of the range for this analysis, such as K, Ca, Mg, S, P, Cd and Pb.

The sample was mounted on a piezo nanopositioner stage, and was raster scanned through the focused beam in vacuum, with the transmission signal and the entire X-ray fluorescence spectrum recorded simultaneously at each pixel. The transmission signal was acquired using a fast-read-out, electron-multiplying CCD camera (Andor Ixon, UK) coupled to a phosphor-screen-based visible-light converting system; this allowed for simultaneous detection of brightfield and differential phase contrast signals. The fluorescence signal was recorded by an energy dispersive detector, which consisted of four large-area (30 mm^2) Si-Drift detectors (PNSensor, Germany) placed in an annular back-scattering configuration around the specimen. The LEXRF data acquisition allowed only for qualitative analyses, although detection limits of about 10 ppm for K-absorption edges

were measured (Gianoncelli et al. 2009; Kaulich et al. 2009), ensuring the chemical sensitivity of the set-up.

The step size was set to 1 μm, and the dwell time per pixel to 17 s to ensure adequate counting statistics. The recorded spectra were normalised for the X-ray-beam fluctuations (beam-intensity current). Element maps were generated from the 3D LEXRF original datasets (positions, energy) by spectral filtering for each pixel, using the PyMCA data-analysis software (batch-fitting procedure, Gaussian peak shape, polynomial baseline subtraction) (Solé et al. 2007).

Results

Visible light and UV fluorescence microscopy

The different tissues of the *N. praecox* leaves were easily distinguished in the cross-sectional images (Fig. 1a and b) that is, the upper and lower epidermis with large vacuolated epidermal cells, palisade mesophyll, spongy mesophyll and vascular bundles. These microscopy images revealed the presence of a layer of purple pigmented sub-epidermal cells in both the adaxial and abaxial leaf regions. A notable morphological heterogeneity was observed within the palisade and the spongy mesophyll tissue under UV excitation (Fig. 1b) indicating localized differences in cell functions within the tissues.

The thickness of the leaf cross-sections (12 μm) was chosen as a compromise between the need to provide an efficient signal-to-noise ratio in FTIR analysis without any saturation in any of the spectral domains considered and to maintain the main morphological features of the sample as much as possible intact (Fig. 1c). Upon inspection of the dried leaf cross-sections, the most preserved areas as indicated by green colour of the chloroplast-containing mesophyll cells and anthocyanin containing vacuoles in the sub-epidermal cells on the visible light images (Fig. 2a) were chosen for FTIR mapping. Nonetheless, some of the vacuoles were lost for some epidermal cells due to the small thickness of the sections and due to the fact that the cryotome sectioning is actually freeze-fracturing creating irregular sections' surface. Acknowledging this, the acquired IR and Zn X-ray fluorescence signals are representative of the cell wall and cytosolic components, but not of the vacuoles.

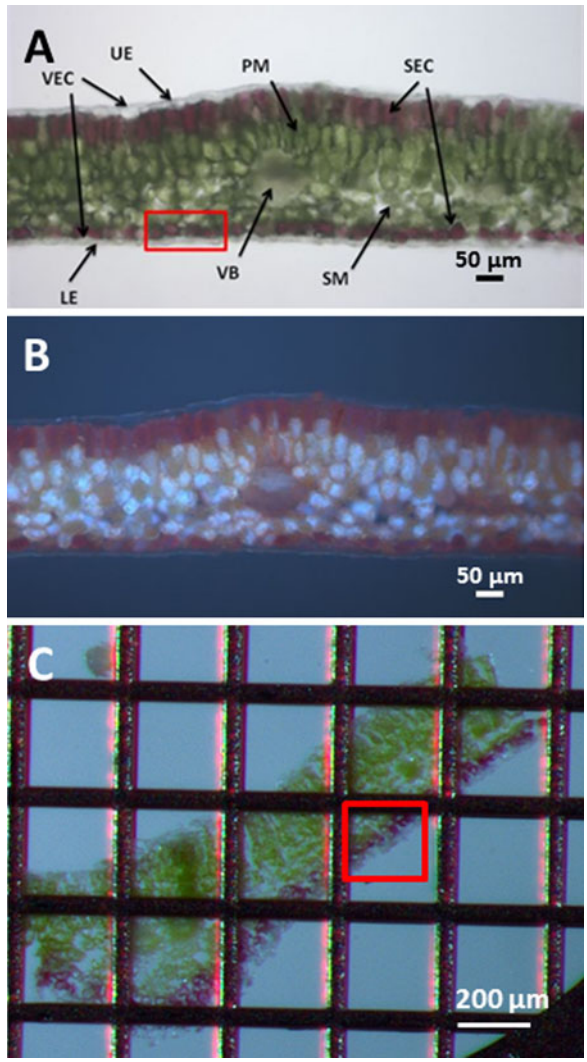

Fig. 1 Leaf cross-sections of field-collected *N. praecox* plants. The *squares* indicate regions of interest. **a** Detailed morphology of the hand-cut leaf cross-section, **b** Autofluorescence of the hand-cut leaves under UV excitation (365 nm), **c** Cryotome cut (12 μm) and freeze-dried leaf cross-section mounted on the transmission electron microscopy grid. LE, lower epidermis; PM, palisade mesophyll (i.e. adaxial side); SM, spongy mesophyll (i.e. abaxial side); SEC, sub-epidermal cells; UE, upper epidermis; VB, vascular bundle; VEC, vacuolated epidermal cells

FTIR microspectroscopy

The assignments of the major and representative bands that can be identified in the spectra from the FTIR micro-spectroscopy are listed in Table 1, in agreement with the published literature. The complexity of the *N. praecox* infrared leaf spectra makes a complete band

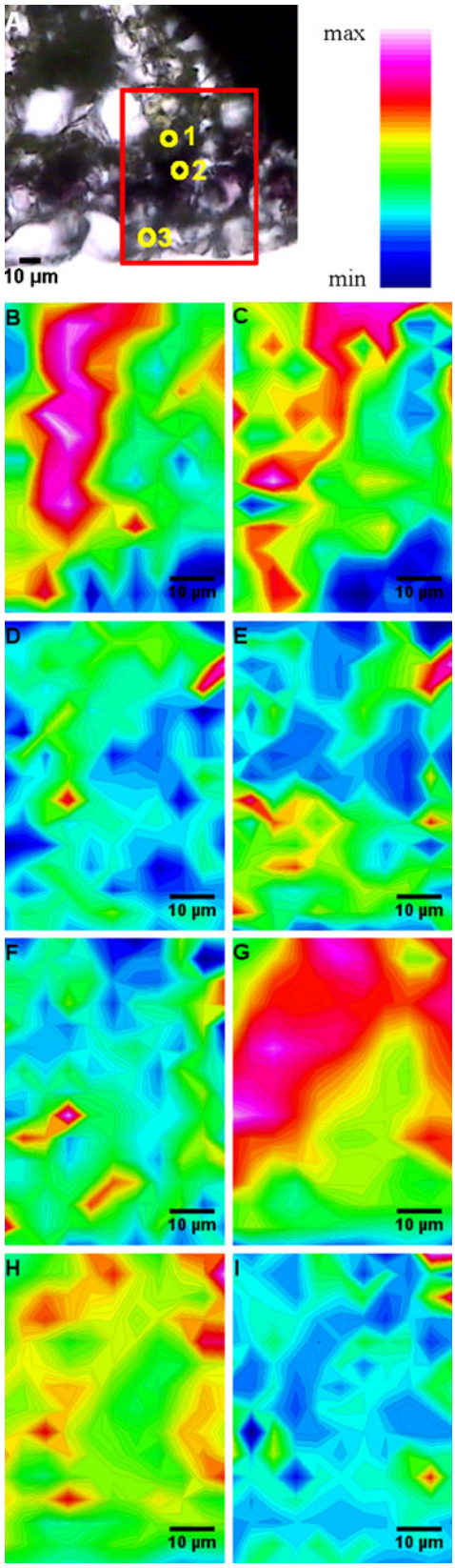

◀ **Fig. 2** Synchrotron radiation FTIR chemical mappings under peak areas of the leaf cross-section of field-collected *N. praecox* within mesophyll (1), sub-epidermal (2) and epidermal (3) cells. **a** Visible light microscopy of the selected region (X15), **b** Lipids (2,928 cm^{-1}; mapping baseline: 2,980–2,820), **c** Ester band (1,735 cm^{-1}; mapping baseline: 1,751–1,715), **d** Amide I (1,655 cm^{-1}; mapping baseline: 1,670–1,620), **e** Amide II (1,545 cm^{-1} mapping baseline: 1,570–1,480), **f** Lignin (1,515 cm^{-1}; mapping baseline: 1,530–1,490). **g** Total carbohydrates (1,010 cm^{-1}; mapping baseline: 1,180–900), **h** Cellulose (1,250 cm^{-1}; mapping baseline: 1,288–1,214), **i** Pectin (1,014 cm^{-1}; mapping baseline: 1,025–1,000). The bands were assigned according to the literature (for details see Table 1)

assignment difficult, as many of the bands were buried or overlapped by others, and therefore many functional group contributions had to be taken into account simultaneously.

Chemical mapping

The distributions and relative concentrations of the chemical functional groups associated with the *N. praecox* leaf-tissue sub-structures mapped are represented in Fig. 2. The colour maps generated were derived from a region marked in the visible images (Fig. 2a**,** rectangle) using particular spectral features to reveal the specific functional groups across the area. In particular, spatial distribution of four larger functional groups, namely lipids, proteins, aromatic compounds and carbohydrates was studied in detail. All of the infrared maps showing different patterns in terms of functional group partitioning support the concept that the mapping and imaging obtained are based on real chemical discrepancies for the different areas of the samples, and not only on changes in the total absorbance of the spectrum.

Lipids

The dominant absorption bands of the lipids are in the region 3,000–2,800 cm^{-1}, and they were assigned to asymmetric and symmetric stretching vibrations of the CH_3 (2,958 cm^{-1} and 2,874 cm^{-1}, respectively) and CH_2 (2,927 cm^{-1} and 2,852 cm^{-1}, respectively) acyl-chain groups of alkanes. In addition, a strong absorption band centred at ~1,735 cm^{-1} represents mainly the stretching vibration of the carbonyl group C=O, in the ester linkage, and indicates that the majority of the esters were saturated. Figure 2b shows the chemical image under area at 2,927 cm^{-1}, showing that lipids are mostly located in specific cells in the sub-

Table 1 Major absorbance bands present in the spectrum of *N. praecox* cells in the 1,800–800 cm^{-1} region. The letters of the first column refer to the bands labelled in the spectrum (Fig. 3). For clarity, the references relating to a compound are only mentioned once. With ν, stretching vibration; δ, bending vibration; ω, wagging vibration; s, symmetric; as, asymmetric

Band	Wavenumber (cm^{-1})	Assignations	Main compounds/ Comments/ References
A	≈ 1,750–1,705	ν(C=O), ν(COO^-)	Carboxylic ester or acetyl groups from ester, fatty acids (Dokken et al. 2005), lignin (Faix 1992), pectin (Vogel et al. 2002), and various polysaccharides
B	≈ 1,655	ν(C=O), ν(C-N)	Mainly from protein (amide I band) (Nelson 1991; Naumann 2000; Ivanova and Singh 2003; Dokken et al. 2005)
C	≈ 1,635–1,615	ν(C=C), ring, $\nu_{as}(COO^-)$	Aromatic system (Stewart 1995; Naumann 2000; Dokken et al. 2005; Schulz and Baranska 2007), protein, pectin
D	≈ 1,605–1,590	$\nu_{as}(COO^-)$, ν(C=C), ν(C=O), ring, $\delta(NH_2)$, $\delta(NH_3)$, ν(C–N)	Carboxyl/ acidic groups from pectin (McCann et al. 1994; Séné et al. 1994; Coimbra et al. 1998; Kačuráková et al. 2000; Kačuráková and Wilson 2001; Jones et al. 2005) or from ligands (Cabaniss et al. 1998; Yang and Hungchen 2002), aromatic systems (quadrant ring vibration) such as lignin, nitro groups (Naumann 2000; Pawlukojc et al. 2005; Grube et al. 2008)
E	≈ 1,565	ν(C=C), ν(C-H), ring	Aromatics, proteins
F	≈ 1,545	ν(C-N), δ(N-H), ν(C-H)	Mainly from protein (amide II band)
G	≈ 1,515	ν(C=C), ν(C=O), ring	Aromatic system (semi circle ring stretch) from lignin (Faix 1992; Himmelsbach et al. 1998)
H	≈ 1,460–1,400	$\nu_s(COO^-)$, $\delta_{as}(C\text{-}H)$, $\delta_{as}(CH_2)$, $\delta_{as}(CH_3)$, ν(C-N)	Carboxyl groups from pectin, aliphatic and alicyclic groups from lignin, various polysaccharides (Séné et al. 1994; Kačuráková et al. 2000; Galichet et al. 2001; Dokken et al. 2005; Schulz and Baranska 2007), amine groups from proteins
I	≈ 1,370	ν(C-C), ν(C=C), ν(C-H), $\delta_s(CH_2)$, $\delta_s(CH_3)$, $\delta_s(CH)$	Pectin, proteins, lipids, lignin, various polysaccharides (cellulosic and hemicellulosic compounds: Séné et al. 1994; Kačuráková et al. 2000; Galichet et al. 2001)
J	≈ 1,325	ν(COO^-), ν(C-H), δ(N-H), ν(C-O)	Carboxyl groups from ligands, proteins, various polysaccharides (cellulosic compounds)
K	≈ 1,300–1,260	$\nu_{as}(COO^-)$, ν(C-C), ν(C-O), ν(C=O), ν(S=O)	Carboxyl groups from ligands, pectin, lignin and various polysaccharides (including sulphuric polysaccharides; Chakravarty et al. 2010)
L	≈ 1,260–1,200	ν(C-C), ν(C-O), ν(C=O), ν(C-N), δ(N-H), $\nu_{as}(PO_2)$, ν(P=O)	Lignin, proteins (amide III), nucleic acids (Stewart 1995; Naumann 2000; Dokken et al. 2005) and various polysaccharides
M	≈ 1,155	$\nu_s(COC)$, ν(C-C), ring	Various polysaccharides (mainly cellulosic compounds; Bonetta et al. 2002)
N	≈ 1,106	ν(C-O), ν(C-C), δ(CHO), $\nu_{as}(COC)$, ring	Pectin
O	≈ 1,070	ν(C-O), ν(CHO), $\nu_{as}(COC)$, ν(C=C), δ(CHO)	Various polysaccharides (hemicellulose in particular; Hori and Sugiyama 2003)
P	≈ 1,045	ν(C-O), ν(C-C), ν(C=C), ν(COC), ring	Pectin, various polysaccharides (cellulose, hemicellulose, β-glucan), also suberin or cutin (Stewart 1995)
Q	≈ 1,025	ν(C-O), ν(C-C), ν(C=C), ν(COC), ν(C=O), ring	Various polysaccharides (especially non structural carbohydrates such as starch)
R-U	≈ 1,020–800	ν(C-O), ν(COC), [ν(C-C), ν(C=C), ring, δ(CHO), δ(C=O), $\delta(CH_2)$, $\delta(CH_3)$, δ(C-H), $\omega(CH_2)$, ω(C-H), $\nu_s(COS)$, ν(C-S) $\nu(PO_3)$, ν(P-O)…]	Pectin, various polysaccharides (phytate (He et al. 2006), sulfated polysaccharides (Harris and Turver 1970; Singh et al. 2006; Chakravarty et al. 2010), lignin…)

epidermis and the mesophyll, and in between and/or in cells of the epidermis, the cells of which are clearly separated by the lipid content of their cell walls. In Fig. 2c the chemical image of the area at ~1,735 cm^{-1} is representative of the major lipid and the pectin distributions. Although fully consistent with Fig. 2b, it is less sensitive to the lipid contributions and demonstrates that part of the pectin or endogenous lipid components is sufficient to induce differences between the maps. Indeed, more methyl, carbonyl or phenolic esters are found in the epidermis than in the sub-epidermis and mesophyll, in which esters are confined to specific cells. The cell walls are less visible in the epidermal layer, as the esters are also inside the cells. Both Fig. 2b and c demonstrate the chemical heterogeneity present inside and within all of the layers and in between the different components indicated by the same molecular groups.

Proteins

The proteins images were generated from the peak under area of the absorption bands specific to amide I, at 1,655 cm^{-1} (Fig. 2d), and amide II, at 1,545 cm^{-1} (Fig. 2e). These two images show important differences, as the amide II band arises from complex vibrations that also involve multiple functional groups and overlap with bands coming from many other groups, such as aromatics, and carboxyl or nitro groups. Therefore, the amide II band is less representative of protein localisation. Figure 2d shows that proteins are present inside the cells of the epidermis, sub-epidermis and mesophyll, with a higher proportion and a co-localisation with the esters in the mesophyll (Fig. 2c). Figure 2e shows that the contribution of the aromatic, carboxyl and/or nitro groups to the makeup of the amide II chemical structure is especially important inside and around the cells of the epidermis, although heterogeneously. These also decrease from the sub-epidermis to the mesophyll.

Aromatic compounds

Figure 2f shows the chemical image under area at 1,515 cm^{-1}, which results from semicircle ring stretch and which in plants has been attributed univocally to lignin. Lignin is located mainly in the cell walls and in large gap junctions between the lower epidermal cells, partially in the walls of the sub-epidermis, and to a lesser extent in the mesophyll. Spatial heterogeneity in these layers can again be observed.

Carbohydrates

The major features of carbohydrates are represented in the 1,180–900 cm^{-1} domain and are mainly due to C-O stretching vibrations. The spectra of carbohydrates are not fully understood in a complex plant system such as the leaf, as these show band patterns with strong features for both structural (cellulose, hemicellulose) and non-structural (starch) carbohydrates. Figure 2g displays the image under peak area centred at ~1,010 cm^{-1}, which represents the total carbohydrate contribution. As expected, the total level of carbohydrates is extremely high in the mesophyll, and then decreases down to the lower epidermis. Again, particular cells in the sub-epidermis and mesophyll appear to contain fewer carbohydrates. More specifically, Fig. 2h shows the chemical structural content under peak area at 1,250 cm^{-1}, of cellulosic material, the concentration of which is higher in the sub-epidermis and mesophyll, and lower in the epidermis. This is due to the fact that the cellulosic component β-glucan is present in higher proportions in the mesophyll cells, and contributes consequently to the infrared image, although pure cellulose is proportionally more important in the epidermis. Figure 2i shows the chemical image under peak area at 1,014 cm^{-1} for pectin, and shows some expected correspondence with Fig. 2c. Pectin polysaccharides are found in and in between the cells of the epidermal and sub-epidermis layers. Again, some heterogeneity in its distribution, with cells showing almost no pectin, may also be observed in the mesophyll.

Biochemical differences between epidermal, sub-epidermal and mesophyll cells

The spectra patterns of the different structures are markedly specific to the area probed. Figure 3 shows the average of spectra (minimum 5) from mesophyll, sub-epidermal and epidermal cells specifically (Fig. 2a) for the fingerprint region (1,800–800 cm^{-1}) since differences in the intensities and precise peak positions lead to a distinct spectral profile, in agreement with observations reported.

The mesophyll is characterised by the highest protein content, in comparison with the epidermis and

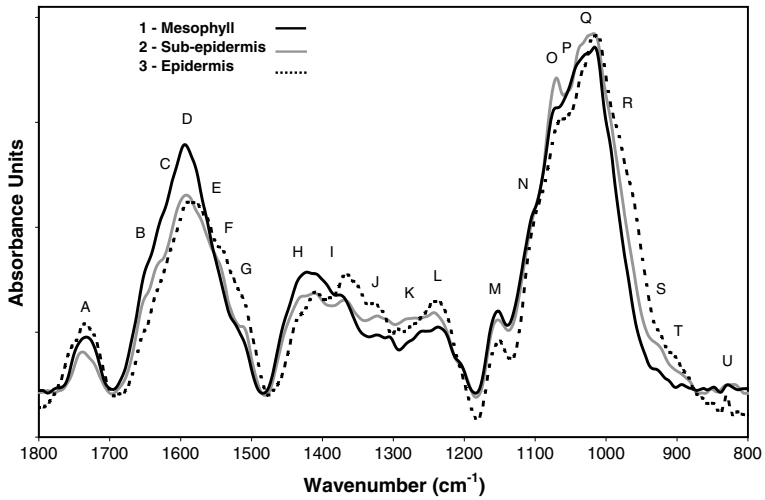

Fig. 3 Representative FTIR spectra of the selected region within mesophyll (1), sub-epidermal (2) and epidermal (3) cells of field-collected *N. praecox* leaves. For accurate comparison, the spectra were normalised using a vector-normalisation algorithm. The letters highlight the most prominent absorption features of the particular carbohydrate features (protein, lipid, starch) and refer to the Table 1

sub-epidermis, as demonstrated by the clear contributions of amide I (1,655 cm^{-1}: ν(C=O), ν(C-N)) and amide II (1,545 cm^{-1}: ν(C-N), δ(N-H)), and especially by the most intense broad absorption band centred at 1,595 cm^{-1}. This peak can be attributed mainly to the quadrant ring stretch of lignin or phenolic compounds (chlorophyll, anthocyanin) (1,595 cm^{-1}: ν(C=C)), although as suggested by the clear shoulders, it can also be composed of a high proportion of acidic groups of pectin and free carboxylate anions (1,600 cm^{-1}: $\nu_{as}(COO^{-})$). Lignin is present in the mesophyll, as confirmed by its characteristic band at 1,515 cm^{-1} (ν(C=C), semicircle ring), although at significantly lower amounts than in the epidermis and the sub-epidermis. The epidermis is characterised by a broad band centred at 1,585 cm^{-1}, a shift indicating that the chemistry of this layer is completely different from the mesophyll and sub-epidermal layers, which contain less phenolic and/or ring functional groups and more proteins. Besides the above-mentioned acidic group of pectin, free carboxylate anions, lignin and/or phenolic compounds, the band is composed of several others groups, which mainly arise from aromatic, carboxylic and/or nitroaromatic free anions, as indicated by the contributions at 1,585 ($\nu_{as}(COO^{-})$, ν_{s}(C=O), ν(C=C), ring, ν(N=O), $\delta(NH_2)$, $\delta(NH_3)$) and 1,565 cm^{-1} (ν(C=C), ν(C-H), ring).

As already mentioned, the region relative to structural and non-structural carbohydrates (1,180–900 cm^{-1}) is extremely complex. However, strong absorption at 1,155 cm^{-1} can be attributed to the cellulosic components (ν(COC), ring), for which the contribution is higher in the epidermis compared to the mesophyll or sub-epidermis, and confirmed by the feature at 1,368 cm^{-1} ($\delta_s(CH_3)$, $\delta_s(CH_2)$ ν(C-C)). Moreover, the bands at 1,420 (ν(COO^{-})), and 1,041 cm^{-1} (ν(COC), ring) can be assigned to β-glucan, the proportions of which are highest in the mesophyll. Also, starch is distributed in higher proportions in the mesophyll, as indicated by the band at 1,025 cm^{-1} (ν(COC), ν(C=O), ν(C-C)). Other hemicellulosic components are present at higher levels in the sub-epidermal layer, as reveal by the peak at 1,070 cm^{-1} (ν(C-O), ν(C-C), δ(COH), ν_{as}(COC)).

The pectin proportion is very high in the epidermal layer, as reflected by the infrared features at ~1,368 ($\delta_s(CH_2)$, $\delta_s(CH_3)$, ν(C=C)), 1,106 (ν(C-O)), ν(C-C), δ(OCH), ring), 1,014 (ν(C-O)), ν(C-C), δ(COH), ring) and 970 (δ(C=O)). Furthermore, the features at 1,435 cm^{-1} and 1,415 cm^{-1} (ν(COO^{-}), δ(CH)) highlight the high proportion of carboxyl groups from pectin in the epidermis compared to the sub-epidermis or mesophyll. The important pectin contribution to the epidermis is also characterised by the high dissymmetry of the peak that is commonly attributed to lipid esters. Although showing a clear maximum at 1,735 cm^{-1} (ν(C=O)), which results from the carboxylic ester or acid groups of lipids, this peak also has clear contributions at 1,748 cm^{-1} and 1,720 cm^{-1}, which are characteristic of the carboxyl and phenolic ester of pectin, respectively. Moreover, it is composed of free carboxylate groups (1,710 cm^{-1}: ν(C=O), ν(COO^{-})) from the ligands, although only for the epidermal layer.

Of particular interest in the epidermal cells is high absorption at 1,241 cm^{-1} (ν(C-O), ν(C-N), δ(N-H), $\nu_{as}(PO_2)$, ν(P=O)), which is mainly associated with

phenolic groups of various polysaccharides, nucleic acids and phosphate groups. The importance of phosphorus groups is strengthen by the two linked absorptions at 990 ($\nu(PO_3)$ ν(P-O)) and 830 cm^{-1} ($\nu(PO_3)$, ν(P-O), δ(P-H), ω(C-H)), features that are strong for the epidermal layer, and to a lesser extent for the mesophyll, and which are characteristic for phytate, and stand for metal phosphate compounds. The sharp peak at 830 cm^{-1} was shown to be invariant in all of the phytate complexes and was extremely representative of those compounds. As well as being restricted to the epidermal cells, the presence of nitroaromatic compounds (such as histidine) is demonstrated by the characteristic band at 1,351 cm^{-1} ($\delta(NH_2)$, $\delta(NH_3)$).

Another point to be noted is the presence of sulphur groups, as revealed by the bands at 1,390 (ν_{as}(S=O)), 1,260 cm^{-1} (ν_{as}(S=O), ν_s(S=O)), and ~850–840 and 832 cm^{-1} (both ν_s(COS)), which can be related to sulphuric polysaccharides, and at 865 cm^{-1} (ν(C-S)) to thiol compounds (glutathione). Again, these frequencies can overlap strongly with vibration modes of other groups, can show significant shifts in complexes, and are usually of weaker intensities in comparison with other group vibrations. All of the glutathione compounds showed absorption at 1,298 cm^{-1}, which is related to their amine groups, although the representative metal-glutathione absorption occurs below 650 cm^{-1}, which was out of range for this analysis. While present in all layers, these features are clearer in the lower epidermis, and especially the band at 865 cm^{-1}, a marker for phytochelatin.

X-ray microspectroscopy

The morphological analysis of the *N. praecox* leaf cross-sections in the lower-epidermal region (Fig. 4a) at cellular and sub-cellular levels was performed in scanning transmission mode. The structures of the

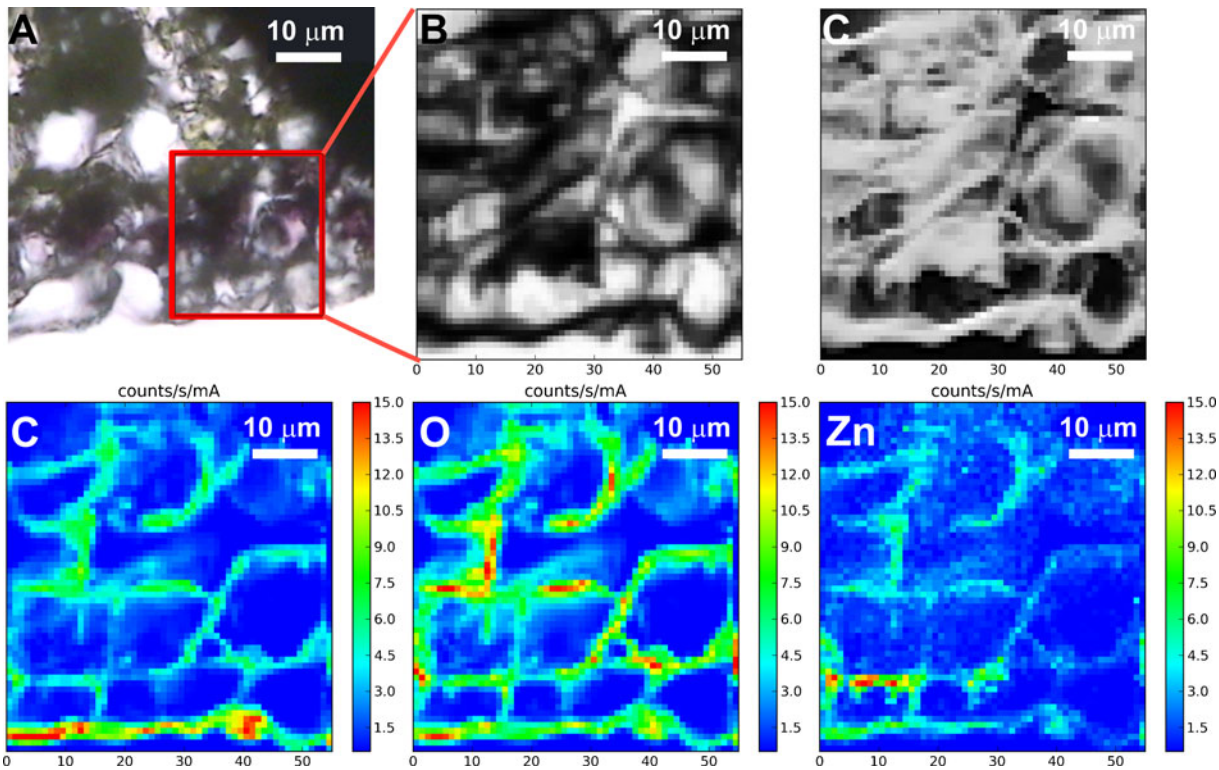

Fig. 4 Qualitative element maps (55×60 µm) of the selected leaf cross-section of field-collected *N. praecox* in the lower-epidermal-cell region, simultaneously acquired with the TwinMic X-ray scanning microscope in transmission and LEXRF modes. Excitation energy: 1,216 eV, step size: 1 µm, dwell time per pixel: 17 s. *Top panels*: **a** Visible light microscopy (X15), **b** Brightfield (absorption) image, **c** phase contrast image. *Bottom panels*: Element distribution maps (C, O, and Zn, normalized: counts/s/mA). Note that in epidermal cells the vacuoles were not retained in the specimen, so elemental maps reflect distribution of elements mainly in the cell walls and the cytoplasm

epidermis, the sub-epidermis and mesophyll regions on visible light figures can be easily associated with the structural network of the cells, cell walls, and cell junctions observed on brightfield and differential phase contrast images (Fig. 4b and c; top panels) and complemented with the acquisition of the LEXRF maps, which directly link the element partitioning within the different cellular sub-structures to their physio-morphological and metabolism characteristics.

The LEXRF investigation allowed for the resolution of the distributions of C, O, and Zn and their relative concentrations within the different structures in the *N. praecox* leaves. Figure 4 (bottom panels) illustrates the element distribution colour maps, derived from the region indicated by the rectangle (55×60 μm). The C and O maps represent the physiological backbone of the elements that are primarily involved in the leaf structures, which arise from the major macromolecules present in the cells, such as carbohydrates and lipids. The elemental maps revealed high contributions of C and O in the cell walls, and a lower proportion inside the cells, with the partitioning of C and O fully correlated. The elemental maps of Zn revealed their primary localisation in the epidermal cells, whereas in the sub-epidermis and mesophyll, the relative concentrations of Zn were considerably lower.

Discussion

Metal hyperaccumulating plants, with their exceptional abilities to withstand metal concentrations in their tissues that are lethal for other plant species, represent excellent models for studying metal accumulation and tolerance mechanisms (Clemens 2001). Metal accumulation in mature leaves of metal-hyperaccumulating *Noccaea* species, particularly Zn, is preferentially occurring in the epidermal cells, more precisely in vacuoles of large epidermal cells (Küpper et al. 1999, 2004; Vogel-Mikuš et al. 2008a, b). It is widely accepted however, that high Zn amount can be also found in epidermal apoplast (Küpper et al. 1999; Vogel-Mikuš et al. 2008a). Metal concentrations in the symplast of epidermal cells in field-collected *N. praecox* leaves reach up to 150,000 μg g^{-1} Zn, 1,000 μg g^{-1} Ni and 1 600 μg g^{-1} Cd, whereas their apoplast retention ratio calculated relatively to the symplast concentrations differs depending on the metal in question with 0.26 of symplast Zn, 1.49 of symplast Cd and 0.28 of symplast Ni (Vogel-Mikuš et al. 2008b). There is nonetheless little information on the macromolecular composition of the non-vacuolar compartments in metal hyperaccumulating plants. As argued previously, due to low thickness of the sample required for the purpose of FTIR analysis and consequent loss of the vacuoles from large epidermal cells during cryo-sectioning, the vacuolar Zn localization could not be confirmed with LEXRF in the examined sections. We have therefore focused on the spatial differences in the biochemical constitution of the non-vacuolar cell compartments within *N. praecox* leaves.

Metal (Cd and Zn) distribution pattern in *N. caerulescens* leaves was suggested to be mainly predisposed by the number of metal transporters present in different cell types, namely TcZNT5, which were reported to be much more abundant in the plasma membrane of epidermal storage cells than in the other cell types, making large vacuolarised epidermal cells the main sink for Zn storage. A higher number of metal transporters in plasma membrane were also related to increased levels of metal sequestration in the vacuole (Leitenmaier and Küpper 2011). Of importance, dynamic processes of metal homeostasis affecting distribution between apoplast and symplast involve metal influx from apoplast to the symplast and further sequestration in the vacuoles, as well as metal efflux from the symplast back to the apoplast (Ebbs et al. 2009). Therefore leaf metal distribution patterns and metal tolerance may not solely depend on the number of specific transporters present in the membranes of particular cell types but also on the biochemical composition of particular cell types.

Zn is known to be transported from root to shoot of metal hyperaccumulating plants mainly as complexes with histidine or organic acids. Zn is also reported present in xylem sap as free hydrated ion, which is mainly dependent on the pH. Whether metal-ligand complexes are dissociated when they enter the mesophyll symplast is, however, not known. After xylem unloading to the mesophyll, metals are transported with mass flow to water evaporation sites. Along their pathway they first interact with the cell wall components and then enter the symplast through specific metal transporters. In leaf cells Zn was found to be coordinated mainly with O-ligands, which indicates a primary role of carboxyl and hydroxyl groups in metal detoxification (Sinclair and Krämer 2012). Metals in high concentrations are known to compete for the available binding

sites and to displace essential cations, such as Ca, Mg, K and Na, from the cell wall and intracellular components. The binding of metals to cellular components might be quite specific and dependent on their composition, on the metal type and its form (ionic/ non-ionic), electronegativity, size and concentration, on the presence of other ions, and on the pH and cation exchange capacity of the plant cell (Sattelmacher 2001). In particular, metal binding to the cell wall components depends mainly on the amount of free carboxyl, hydroxyl, thiol and phosphate groups available, with a clear relation in between the charge and electronegativity of the metal ion and the number of negative charged groups, which also define the strength of the complex ligand-metal (Ke et al. 1994). Therefore, less free carboxyl and hydroxyl groups should be present in mesophyll than in epidermal cell walls, making mesophyll cells more inert for metal binding which may reduce metal uptake into the mesophyll symplast. This is supported by the FTIR microspectroscopy data which indicate that in epidermal cells of field collected *N. praecox* there is a higher amount of carboxyl groups coming from different compounds, such as pectic, and proteinic or organic and amino or free acids than in the mesophyll cells. The specific occurrences of free carboxyls in the epidermis, where LEXRF maps reveal the presence of Zn, strengthen their potential role in metal sequestration. In particular Zn enrichment in epidermal cells was positively correlated with pectin compounds. Structurally complex pectic polymers have important function in cell wall remodelling, and in the control of the cell wall porosity, ionic environment, crosslinking, cellular adhesion, and consequentially influence plant growth (Somerville et al. 2004; Knox 2008). Under stress, structural carbohydrates (cellulose) mostly associated with pectins can evolve in response to metal-ion influx. Pectin methylesterases can remove some methyl groups from the cell walls components, making the carboxyl groups available for coordination with Ca^{2+} (and other divalent cations, with binding affinities that differ widely), to form inter-chain salt bridges (Marry et al. 2006). The cations are held in the interstices of adjacent polysaccharide chains and are complexed by oxygen. The structure of the chain aggregates has been described as the "egg-box" model, emphasizing the relevance of their geometry for the accommodation of the divalent cations in-between (Grant et al. 1973). Zn has been shown to strongly interact with free carboxylate groups of pectin gels, while displacing the monovalent cations (Na^+, K^+). The shifts observed in the FTIR spectra (~1,600, 1,420 and 1,018 cm^{-1}) have been explained by the formation of multidentate complexes between pectin carboxyl groups and metals (Wellner et al. 1998; Kačuráková and Wilson 2001), again, in agreement with the "egg-box" model. Interactions of different metals with pectins may either occur by exchange of metal ions with Ca, or by adsorption to any protonated negative charges within the system, with pectic carboxyl groups being the predominating binding sites (Nari et al. 1991; McKenna et al. 2010). Consequently, the crosslinking of pectin molecules by cations, together with contributions from the cellulosic compounds, from phosphoric and other organic acids (Owens et al. 1952) may have an important role in the organisation, nature and functions of polysaccharides in plant cell walls. Particularly, the involvement of cell walls pectin was previously linked to binding of Pb and Cu in different plant species and/or different populations of the same species (Krzesłowska et al. 2009; Colzi et al. 2011). Pectin components might therefore serve as key metal entrapping molecules preventing metal diffusion back into the more metabolically active and more sensitive mesophyll symplast.

FTIR data also showed an increased proportion of lignin in the epidermis versus the mesophyll. Lignin biosynthesis genes can be highly up-regulated by Zn and Cd treatments in the roots of *N. caerulescens* (van de Mortel et al. 2006, 2008), and increased lignification has been observed in soybean roots treated with Cd (Yang et al. 2007), suggesting metal-induced modifications of the cell wall composition to prevent an excess efflux of metals from the vascular cylinder more efficiently than in non-accumulating *A. thaliana* (van de Mortel et al. 2006; Lequeux et al. 2010). The lignification process leads to an increase in methyl-esterified pectin, which can affect ion binding, reduce the number of negative charges, and hinder the formation of chain aggregates. Nevertheless, Zn has been reported to interact efficiently with esterified pectin (Wellner et al. 1998), and lignin was demonstrated to effectively bind metals to its phenolic sites via free hydroxyl groups (Guo et al. 2008). Increased lignification of epidermal walls might furthermore prevent metals from leaking from the metal-enriched epidermal cells. In addition to the metal-ion affinity for carboxylic and phenolic groups, the pectin, lignin, proteins and other components are stabilised in the cell walls by intermolecular and intramolecular cross-linking (Thakur et al. 1997; Chabannes et al. 2001). Such strong electrostatic

interactions might favour the 'trapping' of other metal complexes inside the cell wall polysaccharide networks, as for those formed with organic acids or glutathione. Other candidates for metal sequestration, as suggested by the FTIR data are: nitroaromatics, such as histidine, phytochelatins, thiols, such as glutathione, phenolic compounds, such as anthocyanins (seen as purple pigment in subepidermal cells using optical microscopy), and phytic acid. All of these were reported to react with Zn, but their precise involvement in hyperaccumulators still needs further investigation.

Conclusions

Metal hyperaccumulating *N. praecox* is structurally and functionally adapted to tolerate extraordinary high heavy metal levels. We confirmed the hypothesis that structural composition of metal enriched epidermal cells in leaves includes biomolecules involved in metal immobilisation and may as well affect metal partitioning between different leaf tissues. Using a combination of synchrotron-radiation-based microspectroscopic techniques, namely FTIR and LEXRF successively, on the same area of interest, the morphological characteristics of cellular and sub-cellular structures within *N. praecox* leaves can be linked to their biochemical and element compositions. Our results confirm that the application of these highly sensitive spatially resolved complementary imaging techniques is indispensable for providing a better picture of metal sequestration and compartmentalisation in plant tissues in situ, allowing for successive biochemical characterisation without chemical preparation of the sample. Using FTIR, epidermal features were linked to the molecular groups of the lipid, protein and carbohydrate components, and especially to pectin, indicating the possible contribution of the different polysaccharides to metal sequestration in these cells, in agreement with the "egg-box" hypothesis. The results show that a large variety of metal ligands co-exist inside the leaf tissues, which are mainly based on carboxyl and hydroxyl groups, and also on amino, phosphate and thiol groups, indicating a wide variety of physiological mechanisms are involved simultaneously and contribute to the dynamic metal sequestration processes in *N. praecox*.

Acknowledgments This study was supported by Slovenian Research Agency -ARRS [P1-0212 Biology of Plants], the ARRS Young Researchers Programme, and the EU COST 859 research programmes. Beamtime was provided by Elettra and EU support [proposals number 20085258 and 20085261]. CB is acknowledged for a lecture of the manuscripts English.

References

Andrade LR, Leal RN, Noseda M, Duarte MER, Pereira MS, Mourão PAS, Farina M, Amado Filho GM (2010) Brown algae overproduce cell wall polysaccharides as a protection mechanism against the heavy metal toxicity. Mar Pollut Bull 60:1482–1488

Bonetta DT, Facette M, Raab TK, Somerville CR (2002) Genetic dissection of plant cell-wall biosynthesis. Biochem Soc Trans 30:298–301

Cabaniss SE, Leenheer JA, McVey IF (1998) Aqueous infrared carboxylate absorbances, aliphatic di-acids. Spectrochim Acta A 54:449–458

Chabannes M, Ruel K, Yoshinaga A, Chabbert B, Jauneau A, Joseleau JP, Boudet AM (2001) In-situ analysis of lignins in transgenic tobacco reveals a differential impact of individual transformations on the spatial patterns of lignin deposition at the cellular and subcellular levels. Plant J 28:271–282

Chakravarty S, Mohanty A, Sudha TN, Upadhyay AK, Konar J, Sircar JK, Madhukar A, Gupta KK (2010) Removal of Pb(II) ions from aqueous solution by adsorption using bael leaves (*Aegle marmelos*). J Hazard Mater 173:502–509

Clemens S (2001) Molecular mechanisms of plant metal tolerance and homeostasis. Planta 212:475–486

Coimbra MA, Barros A, Barros M, Rutledge DN, Delgadillo I (1998) Multivariate analysis of uranic acid and neutral sugars in whole pectic samples by FT-IR spectroscopy. Carbohydr Polym 37:241–248

Colzi I, Doumet S, Del Bubba M, Fornaini J, Arnetoli M, Gabbrielli R, Gonnelli C (2011) On the role of the cell wall in the phenomenon of copper tolerance in *Silene paradoxa* L. Environ Exp Bot 72:77–83

Dokken KM, Davis LC, Marinkovic NS (2005) Use of infrared microspectroscopy in plant growth and development. Appl Spectrosc Rev 40:301–326

Ebbs SD, Zambrano MC, Spiller SM, Newville M (2009) Cadmium sorption, influx, and efflux at the mesophyll layer of leaves from ecotypes of the Zn/Cd hyperaccumulator *Thlaspi caerulescens*. New Phytol 181:626–636

Eichert D, Gregoratti L, Kaulich B, Marcello A, Melpignano P, Quaroni L, Kiskinova M (2007) Imaging with spectroscopic micro-analysis using synchrotron radiation. Anal Bioanal Chem 389:1121–1132

Eichert D, Lupi S, Perucchi A, Nucara A, Calvani P, Vaccari L, Morgera F, Kiskinova M (2008) Infrared microspectroscopy at SISSI, the ELETTRA Sincrotron Trieste infrared beamline. Synchrotron Radiat News 21:45–50

Ernst WHO (2006) Evolution of metal tolerance in higher plants. For Snow Landsc Res 80:251–274

Faix O (1992) Fourier transform infrared spectroscopy. In: Lin SY, Dense CW (eds) Methods in lignin chemistry, 6. Springer-Verlag, Berlin, pp 83–109

Galichet A, Sockalingum GD, Belarbi A, Manfai M (2001) FTIR spectroscopic analysis of *Saccharomyces cerevisiae* cell walls: study of an anomalous strain exhibiting a pink-colored cell phenotype. FEMS Microbiol Lett 197:179–186

Gianoncelli A, Kaulich B, Alberti R, Klatka T, Longoni A, De Marco A, Marcello A, Kiskinova M (2009) Simultaneous soft X-ray transmission and emission microscopy. Nucl Intrum Meth A 608:195–198

Grant GT, Morris ER, Rees DA, Smith PJC, Thom D (1973) Biological interactions between polysaccharides and divalent cations: the egg-box model. FEBS Lett 32:195–198

Grube M, Muter O, Strikauska S, Gavare M, Limane B (2008) Application of FT-IR spectroscopy for control of the medium composition during the biodegradation of nitroaromatic compounds. J Ind Microbiol Biotechnol 35:1545–1549

Guo X, Zhang S, Shan XQ (2008) Adsorption of metal ions on lignin. J Hazard Mater 151:134–142

Harris MJ, Turver RJ (1970) Sulphates monosaccharides and derivatives: part VIII. Infrared spectra and optical rotations of some glycoside sulphates. Carbohydr Res 15:51–56

Haydon MJ, Cobbett CS (2007) Transporters of ligands for essential metal ions in plants. New Phytol 174:499–506

He Z, Honeycutt CW, Zhang T, Bertsch PM (2006) Preparation and FT-IR characterization of metal phytate compounds. J Environ Qual 35:1319–1328

Himmelsbach D, Khalili S, Akin D (1998) FT-IR microspectroscopic imaging of flax (*Linum usitatissimum* L.) stems. Cell Mol Biol 44:99–108

Hori R, Sugiyama J (2003) A combined FT-IR microscopy and principal component analysis on softwood cell walls. Carbohydr Polym 52:449–453

Ide-Ektessabi A (2007) Applications of synchrotron radiation: microbeams in cell microbiology and medicine. Springer Verlag, Berlin, Heidelberg

Ivanova DG, Singh BR (2003) Nondestructive FTIR monitoring of leaf senescence and elicitin-induced changes in plant leaves. Biopolymers 72:79–85

Jones L, Milne JL, Ashford D, McCann MC, McQueen-Mason SJ (2005) A conserved functional role of pectic polymers in stomatal guard cells from a range of plant species. Planta 221:255–264

Kačuráková M, Wilson RH (2001) Developments in mid infrared FT-IR spectroscopy of selected carbohydrates. Carbohydr Polym 44:291–303

Kačuráková M, Capek P, Sasinková V, Wellner N, Ebringerová A (2000) FTIR study of plant cell wall model compounds: pectic polysaccharides and hemicelluloses. Carbohydr Polym 43:195–203

Kaulich B, Bacescu D, Susini J, David C, di Fabrizio E, Morrison GR, Charalambous P, Thieme J, Wilhein T, Kovač J, Cocco D, Salomé M, Dhez O, Weitkamp T, Cabrini S, Cojoc D, Gianoncelli A, Vogt U, Podnar M, Zangrando M, Zacchigna M, Kiskinova M (2006) TwinMic - A European twin X-ray microscopy station commissioned at ELETTRA. In: Aoki S, Kagoshima Y, Suzuki Y (eds) Proceedings of the 8th International Conference in X-ray Microscopy. Conference Proceedings Series IPAP 7. The Institute of Pure and Applied Physics, Tokyo, pp 22–25

Kaulich B, Gianoncelli A, Beran A, Eichert D, Kreft I, Pongrac P, Regvar M, Vogel-Mikuš K, Kiskinova M (2009) Low-energy X-ray fluorescence microscopy opening new opportunities for bio-related research. J R Soc Interface 6:S641–S647

Ke HYD, Anderson WL, Moncrief RM, Rayson GD, Jackson PJ (1994) Luminescence studies of metal ion-binding sites in *Datura innoxia* biomaterial. Environ Sci Technol 28:586–591

Knox JP (2008) Revealing the structural and functional diversity of plant cell walls. Curr Opin Plant Biol 11:308–313

Krzesłowska M, Lenartowska M, Mellerowicz EJ, Samardakiewicz S, Woźny A (2009) Pectinous cell wall thickenings formation – a response of moss protonemata cells to lead. Environ Exp Bot 65:119–131

Küpper H, Zhao F-J, McGrath S (1999) Cellular compartmentation of zinc in leaves of the hyperaccumulator *Thlaspi caerulescens*. Plant Physiol 119:305–311

Küpper H, Mijovilovich A, Meyer-Klauchke W, Kroneck PMH (2004) Tissue- and age-dependent differences in the complexation of cadmium and zinc in the cadmium/zinc hyperaccumulator *Thlaspi caerulescens* (Ganges ecotype) revealed by X-ray absorption spectroscopy. Plant Physiol 134:748–757

Lang I, Wernitznig S (2011) Sequestration at the cell wall and plasma membrane facilitates zinc tolerance in the moss *Pohlia drummondii*. Environ Exp Bot 74:186–193

Leitenmaier B, Küpper H (2011) Cadmium uptake and sequestration kinetics in individual leaf cell protoplasts of the Cd/Zn hyperaccumulator *Thlaspi caerulescens*. Plant Cell Environ 34:208–219

Lequeux H, Hermans C, Lutts S, Verbruggen N (2010) Response to copper excess in *Arabidopsis thaliana:* Impact on the root system architecture, hormone distribution, lignin accumulation and mineral profile. Plant Physiol Biochem 48:673–682

Lupi S, Nucara A, Perucchi A, Calvani P, Ortolani M, Quaroni L, Kiskinova M (2007) Performance of SISSI, the infrared beamline of the ELETTRA storage ring. J Opt Soc Am B 24:959–964

Ma JF, Ueno D, Zhao FJ, McGrath SP (2005) Subcellular localisation of Cd and Zn in the leaves of a Cd-hyperaccumulating ecotype of *Thlaspi caerulescens*. Planta 220:731–736

Mari S, Lebrun M (2005) Metal immobilization: where and how? In: Tamás MJ, Martinova E (eds) Molecular biology of metal homeostasis and detoxification. Springer, Berlin, pp 273–298

Marry M, Roberts K, Jopson SJ, Huxham IM, Jarvis MC, Corsar J, Robertson E, McCann MC (2006) Cell-cell adhesion in fresh sugar-beet root parencyhma requires both pectin esters and calcium cross-links. Physiol Plant 126:243–256

McCann MC, Shi J, Roberts K, Carpita NC (1994) Changes in pectin structure and localization during the growth of unadapted and NaCl-adapted tobacco cells. Plant J 5:773–785

McKenna BA, Wehr JB, Kopittke PM, Blamey FP, Menzies NW (2010) Novel methods to investigate metal interactions with plant cell walls. In: Gilkes RJ, Prakongkep N (eds) Proceedings of 19th World Congress of Soil Science, Soil Solutions for a Changing World. International Union of Soil Sciences, Brisbane, pp 80–83

McNear DH Jr, Chaney RL, Sparks DL (2010) The hyperaccumulator *Alyssum murale* uses complexation with

nitrogen and oxygen donor ligands for Ni transport and storage. Phytochemistry 7:188–200

Miller LM, Dumas P (2006) Chemical imaging of biological tissue with synchrotron infrared light. Biochim Biophys Acta 1758:846–857

Milner MJ, Kochian LW (2008) Investigating heavy metal hyperaccumulation using *Thlaspi caerulescens* as a model system. Ann Bot 102:3–13

Nari J, Noat G, Ricard J (1991) Pectin methylesterase, metal ions and plant cell-wall extension. Biochem J 279:351–354

Naumann D (2000) Infrared spectroscopy in microbiology. In: Meyers RA (ed) Encyclopedia of analytical chemistry. John Wiley and Sons, Inc., Chichester, pp 102–131

Nelson WH (1991) Modern techniques for rapid microbiological analysis. VCH Publishers, New York

Owens HS, McCready RM, Shepherd AD, Schultz TH, Pippen EL, Swenson HS, Miers JC, Erlandsen RF, Maclay MD (1952) Methods used at western regional research laboratory for extraction and analysis of pectic materials. Bureau of Agricultural and Industrial Chemistry, Agricultural Research Administration, U.S. Department of Agriculture, pp 24

Pawlukojc A, Leciejewicz J, Ramirez-Cuesta A, Nowicka-Scheibe J (2005) L-cysteine: neutron spectroscopy, Raman, IR and ab initio study. Spectrochim Acta A 61:2474–2481

Pongrac P, Vogel-Mikuš K, Kump P, Nečemer M, Tolrà R, Poschenrieder C, Barceló J, Regvar M (2007) Changes in elemental uptake and arbuscular mycorrhizal colonisation during the life cycle of *Thlaspi praecox* Wulfen. Chemosphere 69:1602–1609

Rascio N, Navari-Izzo F (2011) Heavy metal hyperaccumulating plants: how and why do they do it? And what makes them so interesting? Plant Sci 180:169–181

Salt DE, Prince RC, Baker AJM, Raskin I, Pickering IJ (1999) Zinc ligands in the metal hyperaccumulator *Thlaspi caerulescens* as determined using X-ray absorption spectroscopy. Environ Sci Technol 33:713–717

Sattelmacher B (2001) The apoplast and its significance for plant mineral nutrition. New Phytol 149:167–192

Schneider T, Scheloske S, Povh B, Traxel K (2002) A method for cryosectioning of plant roots for proton microprobe analysis. Int J PIXE 12:101–107

Schulz H, Baranska M (2007) Identification and quantification of valuable plant substances by IR and Raman spectroscopy. Vib Spectrosc 43:13–25

Séné CF, McCann MC, Wilson RH, Grinter R (1994) Fourier-transform Raman and Fourier-transform infrared spectroscopy. An investigation of five higher plant cell walls and their components. Plant Physiol 106:1623–1631

Sinclair SA, Krämer U (2012) The zinc homeostasis network in land plants. Biochim Biophys Acta Mol Cell Res 1823:1553–1567

Singh BK, Sharma RK, Garg BS (2006) Cobalt(II) complexes of biologically active glutathione: spectroscopic and molecular modelling studies. Spectrochim Acta A 63:96–102

Solé VA, Papillon E, Cotte M, Walter P, Susini J (2007) A multiplatform code for the analysis of energy-dispersive X-ray fluorescence spectra. Spectrochim Acta B 62:63–68

Somerville C, Bauer S, Brininstool G, Facette M, Hamann T, Milne J, Osborne E, Paredez A, Persson S, Raab T, Vorwerk S, Youngs H (2004) Toward a systems approach to understanding plant cell walls. Science 306:2206–2211

Stewart D (1995) Fourier-transform infrared microspectroscopy of plant tissues. Appl Spectrosc 50:357–365

Thakur BR, Singh RK, Handa AK (1997) Chemistry and uses of pectin – a review. CRC Crit Rev Food Sci Nutr 37:47–73

van de Mortel JE, AlmarVillanueva LA, Schat H, Kwekkeboom J, Coughlan S, Moerland PD, Ver Loren van Themaat E, Koornneef M, Aarts MGM (2006) Large expression differences in genes for iron and zinc homeostasis, stress response and lignin biosynthesis distinguish roots of *Arabidopsis thaliana* and the related metal hyperaccumulator *Thlaspi caerulescens*. Plant Physiol 142:1127–1147

van de Mortel JE, Schat H, Moerland PD, Ver Loren van Theemat E, van der Ent S, Blankestijn H, Ghandilya A, Tsiatsiani S, Aarts MGM (2008) Expression differences for genes involved in lignin, glutathione and sulphate metabolism in response to cadmium in *Arabidopsis thaliana* and the related Zn/Cd-hyperaccumulator *Thlaspi caerulescens*. Plant Cell Environ 31:301–324

Vogel JP, Raab TK, Schiff C, Somerville SC (2002) PMR6, a pectate lyase-like gene required for powdery mildew susceptibility in Arabidopsis. Plant Cell 14:2095–2106

Vogel-Mikuš K, Regvar M, Mesjasz-Przybyłowicz J, Przybyłowicz WJ, Simčič J, Pelicon P, Budnar M (2008a) Spatial distribution of Cd in leaves of metal hyperaccumulating *Thlaspi praecox* using micro-PIXE. New Phytol 179:712–721

Vogel-Mikuš K, Simčič J, Pelicon P, Budnar M, Kump P, Nečemer M, Mesjasz-Przybyłowicz J, Przybyłowicz WJ, Regvar M (2008b) Comparison of essential and non-essential element distribution in leaves of the Cd/Zn hyperaccumulator *Thlaspi praecox* as revealed by micro-PIXE. Plant Cell Environ 31:1484–1496

Vogel-Mikuš K, Pongrac P, Pelicon P, Vavpetič P, Povh B, Bothe H, Regvar M (2009) Micro-PIXE analysis for localization and quantification of elements in roots of mycorrhizal metal-tolerant plants. In: Varma A, Kharkwal AC (eds) Symbiotic fungi. Soil biology 18. Springer-Verlag, Berlin, pp 227–242

Wang D, Mills ES, Deal RB (2012) Technologies for system-level analysis of specific cell types in plants. Plant Sci 197:21–29

Wellner N, Kačuráková M, Malovikova A, Wilson RH, Belton PS (1998) FT-IR study of pectate and pectinate gels formed by divalent cations. Carbohydr Res 308:123–131

Wetzel DL, Eilert AJ, Pietrzak LN, Miller SS, Sweat JA (1998) Ultraspatially-resolved synchrotron infrared microspectroscopy of plant tissue in situ. Cell Mol Biol 44:145–168

Yang J, Hungchen EY (2002) Early salt stress effects on the changes in chemical composition in leaves of ice plant and *Arabidopsis*. A fourier transform infrared spectroscopy study. Plant Physiol 130:1032–1042

Yang YJ, Cheng LM, Liu ZH (2007) Rapid effect of cadmium on lignin biosynthesis in soybean roots. Plant Sci 172:632–639